Inorganic Chemistry

Article

pubs.acs.org/IC

Luminescence Rigidochromism and Redox Chemistry of Pyrazolate-Bridged Binuclear Platinum(II) Diimine Complex Intercalated into Zirconium Phosphate Layers

Eladio J. Rivera,[†] Cindy Barbosa,[†] Rafael Torres,[†] Harry Rivera,[†] Estevao R. Fachini,[†] Tyler W. Green,[‡] William B. Connick,[‡] and Jorge L. Colón*[,†]

[†]Department of Chemistry, University of Puerto Rico, P.O. Box 23346, Río Piedras, P.R. 00931, United States

[‡]Department of Chemistry, University of Cincinnati, P.O. Box 210172, Cincinnati, Ohio 45221-0172, United States

Supporting Information

ABSTRACT: The direct intercalation of a pyrazolate-bridged platinum(II) bipyridyl dimer ($[\{Pt(dmbpy)(\mu\text{-}pz)\}_2]^{2+}$; dmbpy = 4,4′-dimethyl-2,2′-bipyridine, pz^- = pyrazolate) within a zirconium phosphate (ZrP) framework has been accomplished. The physical and spectroscopic properties of $[\{Pt(dmbpy)(\mu\text{-}pz)\}_2]^{2+}$ intercalated in ZrP were investigated by X-ray powder diffraction and X-ray photoelectron, infrared, absorption, and luminescence spectroscopies. Zirconium phosphate layers have a special microenvironment that is capable of supporting a variety of platinum oxidation states. Diffuse reflectance spectra from powders of the blue-gray intercalated materials show the formation of a low-energy band at 600 nm that is not present in the platinum dimer salt. The nonintercalated complex is nonemissive in room-temperature fluid solution, but gives rise to intense blue-green emission in a 4:1 ethanol/methanol 77 K frozen glassy solution. Powders and colloidal suspensions of $[\{Pt(dmbpy)(\mu\text{-}pz)\}_2]^{2+}$-exchanged ZrP materials exhibit intense emissions at room-temperature.

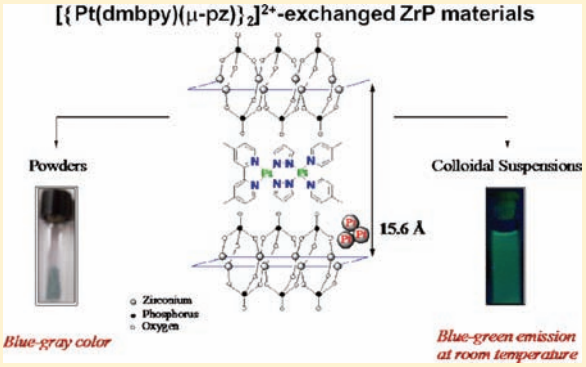

INTRODUCTION

Hybrid materials represent one of the most fascinating developments in materials chemistry in recent years.[1,2] The integration of metal complexes and layered inorganic materials as building blocks, offers tremendous possibilities combining different properties, opening the door for the creation of new advanced multifunctional materials. Metal complexes that have drawn considerable attention over the past few years include platinum(II) pyrazolate monomers and a wide variety of pyrazolate-bridged platinum(II) dimers.[3−9] Cyclometalated Pt(II) complexes have shown attractive applications as dopant phosphorescent emitters in highly efficient organic light emitting devices (OLEDs),[10−15] photocatalytic generation of hydrogen from water,[16] antitumor activity,[17,18] and luminescence-based vapor sensing.[19−21] Other interesting mononuclear and dinuclear Pt(II) complexes that have attracted considerable attention for many of the applications mentioned above are mixed-valence complexes called "platinum blues".[16,22−37] Since Barton and Lippard reported the first crystal structure of cis-diammineplatinum α-pyridonate blue,[34] several dimers, tetramers, and octanuclear complexes with average platinum oxidation states (2.0+, 2.25+, 2.5+, and 3.0+) have been isolated and characterized.[22−26,28−33] Examples of pyrazolate-bridged platinum dimers containing diimine ligands are comparatively rare. Minghetti and co-workers performed the first studies of these systems,[3] and later, Sakai et al. reported the crystal structure of the tetrafluoroborate salt of the $[\{Pt(bpy)(\mu\text{-}pz)\}_2]^{2+}$ cation (pz^- = pyrazolate) that exhibits a basket-like geometry with a relatively short Pt···Pt distance of about 3.231(1) Å.[38]

Recently, we reported that the direct ion-exchange of two monomeric platinum complexes, $[Pt(Me_2bzimpy)Cl]^+$ (Me_2bzimpy = 2,6-bis(*N*-methylbenzimidazol-2-yl)pyridine) and $[Pt(tpy)Cl]^+$ (tpy = 2,2′:6′,2″-terpyridine), into layered inorganic material zirconium phosphate (θ-ZrP)[39−42] produces novel luminescent materials.[43] Those results were consistent with an expansion of the interlayer spacing to about 18 Å to accommodate aggregates of closely interacting platinum complexes. Suspensions and powders of these intercalated materials exhibit distinct absorption and emission spectroscopic signatures characteristic of low-lying metal−metal-to-ligand charge transfer (MMLCT) states resulting from short Pt···Pt spacings.

In this article, we report the first direct ion-exchange of a pale yellow pyrazolate-bridged platinum(II) bipyridyl dimer ($[\{Pt(dmbpy)(\mu\text{-}pz)\}_2]^{2+}$, dmbpy = 4,4′-dimethyl-2,2′-bipyridine; Figure 1) into θ-ZrP layers. The intercalated material has an interesting blue-gray color suggesting the formation of a variety of platinum oxidation states incorporated in a rigid-framework

Received: July 5, 2011
Published: February 16, 2012

   dx.doi.org/10.1021/ic201423q | *Inorg. Chem.* 2012, 51, 2777−2784

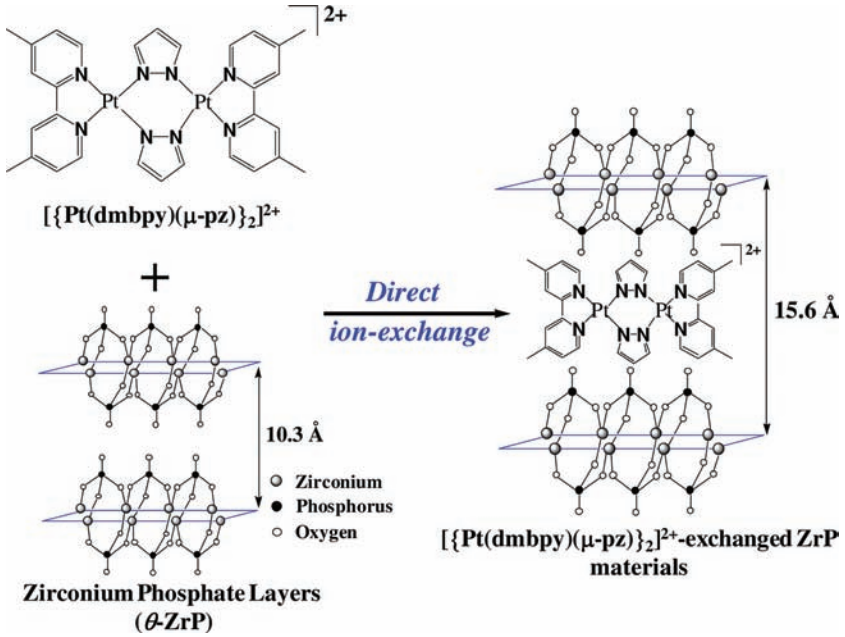

Figure 1. Pyrazolate-bridged binuclear platinum(II) diimine complex ($[\{Pt(dmbpy)(\mu\text{-}pz)\}_2]^{2+}$) intercalated into θ-ZrP.

matrix. Although the nonintercalated dimer is not emissive in solutions at room temperature, powders and colloidal suspensions of the intercalated materials are brightly emissive at room temperature.

EXPERIMENTAL SECTION

Materials. Zirconium oxychloride octahydrate ($ZrOCl_2 \cdot 8H_2O$, 98%) was obtained from Aldrich Chemical Co. Phosphoric acid (H_3PO_4, 85% v/v) was obtained from Fisher. The pyrazolate-bridged platinum(II) bipyridyl dimer ($[\{Pt(dmbpy)(\mu\text{-}pz)\}_2]^{2+}$) and θ-ZrP were synthesized according to established procedures.[3,38,41,42] All other reagents were of spectroscopic grade and were used without further purification.

Intercalation Procedure. ZrP was suspended in 1:1 ethanol:water solutions of $[\{Pt(dmbpy)(\mu\text{-}pz)\}_2](BF_4)_2$ at various $[\{Pt(dmbpy)(\mu\text{-}pz)\}_2]^{2+}$:ZrP molar ratios (1:30, 1:25, 1:10, 1:5, and 1:1) with constant stirring at ambient temperature for 5 days producing $[\{Pt(dmbpy)(\mu\text{-}pz)\}_2]^{2+}$-intercalated ZrP materials with different loading levels. The materials are referenced according to the molar Pt:ZrP concentration ratio of the mixture used in their preparation. The mixture was filtered, and the solid was washed with abundant nanopure water and dried at ambient temperature for 3 days. $[\{Pt(dmbpy)(\mu\text{-}pz)\}_2]^{2+}$-exchanged ZrP blue-gray materials were prepared following the procedure mentioned above. The yellow-brown materials were obtained using the same procedure, but in the presence of sodium dithionite ($Na_2S_2O_4$).

Characterization. X-ray powder diffraction (XRPD) patterns were recorded using a Rigaku Ultima 3 X-ray diffractometer system (Rigaku MSC, Woodlands, TX) with Ni filtered Cu Kα radiation (λ = 1.5418 Å). The X-ray source was operated at 40 kV and 44 mA. Powders of the intercalated materials were mounted on a silicon zero background material. The XRPD patterns were obtained using a high precision and high resolution parallel beam geometry in the step scanning mode with a counting time of 11 s per 0.02°. Scans were recorded in the 2θ range of 2−45°. The interlayer distance (d_{hkl}) of the ZrP materials were determined from the first order diffraction peak using Bragg's law.[44]

X-ray photoelectron spectroscopy (XPS) analyses were performed at the Materials Characterization Center of the University of Puerto Rico using a Physical Electronics PHI 5600 ESCA System equipment. Primary excitation was provided by a Mg anode (Kα radiation, 1253.6 eV) biased at 15 kV and at the power setting of 400 W. The spectra were collected in a fixed analyzer transmission mode on a hemispherical electroanalyzer. The carbon 1s signal at 285 eV was used as the internal reference. High resolution XPS spectra were obtained for the Pt 4f region. Deconvolution was carried out using MultipackXPS software in which a Shirley type background was used. The mixing ratio of Gaussian and Lorentzian functions was fixed at 80:20 and the fwhm values of four components were constrained to 1.93 eV.

Infrared spectra were obtained using a Bruker Tensor 27 infrared spectrophotometer coupled to a Helios Bruker FT-IR microscope.

UV−visible spectrophotometric and steady state luminescence measurements were performed on ethanol:water suspensions (0.008%, w/v) of the intercalated material purged with N_2 (99.999%) for 15 min prior to the analysis. UV−visible absorption spectra were recorded using a Shimadzu UV-2401 PC spectrophotometer. Emission and excitation spectra of Pt(II) complexes-exchanged ZrP colloidal suspensions (0.008% w/v) at different loadings levels were obtained using a Horiba Jobin-Yvon spectrofluorometer (NanoLog FL-322). Glassy solutions at 77 K were prepared using a FL-1013 liquid nitrogen Dewar assembly. For the solid-state samples, the intercalated material was placed in the solid sample holder at 30° from the excitation source and the detector. The emission and excitation spectra were corrected.

Molecular modeling was performed using Spartan Student Physical-Chemistry Edition for Windows v.1.0.1 with the RHF/PM3 semiempirical model for molecular minimization.

RESULTS AND DISCUSSION

Synthesis. Samples of pyrazolate-bridged binuclear platinum(II) diimine complex-exchanged ZrP were readily prepared from suspensions of ZrP in 1:1 ethanol:water solutions of the tetrafluoroborate salt of $[\{Pt(dmbpy)(\mu\text{-}pz)\}_2]^{2+}$. The loading level was controlled by varying the Pt:ZrP molar ratio used in the suspension over a wide range (1:30−1:1), and the materials are referenced according to this concentration ratio. The ZrP underwent a color change from pale yellow to blue-gray during the intercalation process. The color of the resulting powders were increasingly more blue as the loading level was varied from 1:30 to 1:1, ranging from pale gray to intense blue-gray. To determine if $[\{Pt(dmbpy)(\mu\text{-}pz)\}_2]^{2+}$ had undergone any chemical change during or after the intercalation process, FT-IR measurements of the

dx.doi.org/10.1021/ic201423q | Inorg. Chem. 2012, 51, 2777−2784

intercalated materials were performed. As expected, the intensity of the bands associated with the platinum complex increases with loading level (Supporting Information, Figure S1), but no new bands are observed. Overall, the spectra are entirely consistent with the superposition of the spectra of the nonintercalated ZrP and the platinum dimer salt, except for the "lattice" water vibrational bands at 3589, 3508, and 1617 cm^{-1} in unintercalated ZrP which are dramatically reduced in the $[\{Pt(dmbpy)(\mu\text{-}pz)\}_2]^{2+}$-exchanged ZrP IR spectrum, as expected for water displacement upon intercalation of the dimer. These results suggest that no significant chemical change in ZrP or the dimer occurred upon intercalation.

X-ray Powder Diffraction. Figure 2 shows the XRPD patterns for θ-ZrP and the $[\{Pt(dmbpy)(\mu\text{-}pz)\}_2]^{2+}$-exchanged

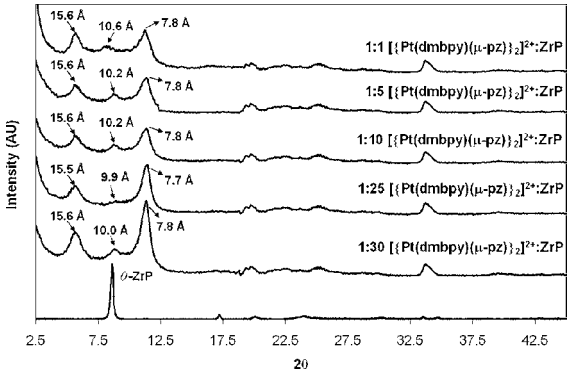

Figure 2. XRPD patterns of 1:30, 1:25, 1:10, 1:5, and 1:1 $[\{Pt(dmbpy)(\mu\text{-}pz)\}_2]^{2+}$-exchanged ZrP and θ-ZrP.

ZrP materials from 1:30 to 1:1 Pt:ZrP molar ratios. The patterns show the formation of mixed phases. At the lowest loading level (1:30 Pt:ZrP) a first-order diffraction peak occurs at an angle corresponding to a 15.6 Å interlayer distance with an intense second-order peak at 7.8 Å. In addition, the diffraction patterns for the 1:30 and 1:25 Pt:ZrP materials show a weaker peak consistent with a 10.0 Å interlayer spacing. The latter feature is in agreement with the interlayer distance expected for ZrP intercalated with one ethanol molecule per formula unit previously observed by Costantino.[45] As the loading level increases from 1:30 to 1:1 Pt:ZrP, this peak loses intensity, indicating the disappearance of the ethanol-intercalated phase because of displacement of ethanol. Since the intercalation process in ZrP is topotactic,[46] the increase in the interlayer distance to 15.6 Å from that of the wet nonintercalated starting material (10.3 Å) indicates that the $[\{Pt(dmbpy)(\mu\text{-}pz)\}_2]^{2+}$ is being intercalated between the layers of ZrP. Assuming that the pyrazolate ligands coordinate in an *exo*-bidentate fashion, forming a puckered six membered ring composed of two Pt atoms and the four pyrazolate N atoms,[38] the van der Waals dimensions of $[\{Pt(dmbpy)(\mu\text{-}pz)\}_2]^{2+}$ are estimated to be 13.3 × 10.5 × 9.3 Å (Figure 3) using SPARTAN.[47] The estimated Pt1···Pt2 distance of 3.661 Å is in reasonable agreement with platinum(II) dimers with a single pyrazolate-bridging ligand (3.43–3.88 Å)[6,48–50] and slightly longer than other dimers with a $\{Pt_2(\mu\text{-pyrazolate})_2\}$ core (3.16–3.49 Å).[5,7,12,38,51,52] The resultant Pt···Pt distance of 3.661 Å is consistent with little-to-no metal–metal interactions.

Since the ZrP layer thickness is 6.6 Å,[53] having the dmbpy ligands perpendicular to the ZrP layers (i.e., the Pt–Pt vector

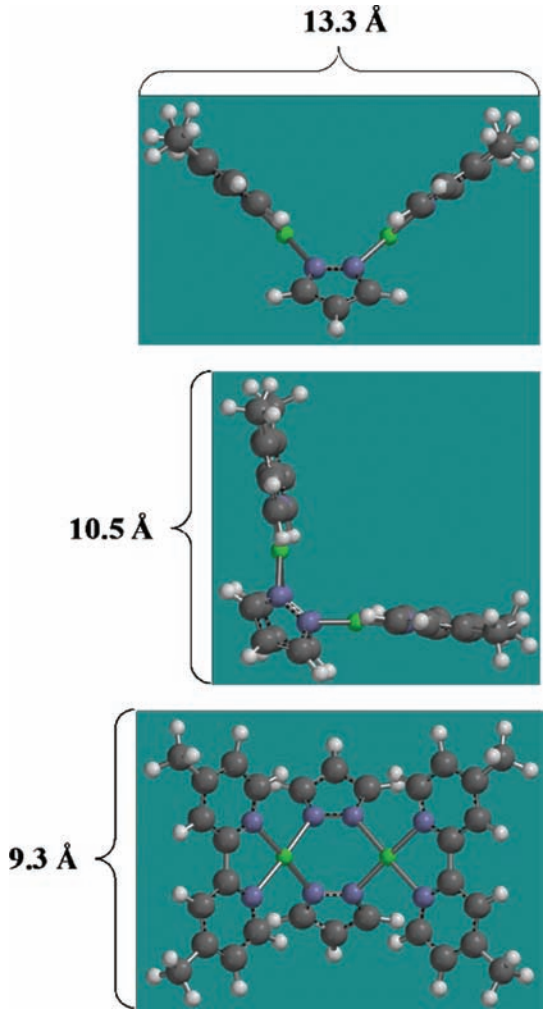

Figure 3. Dimensions of $[\{Pt(dmbpy)(\mu\text{-}pz)\}_2]^{2+}$ as calculated by SPARTAN using RHF/PM3* as a basis set.[43].

parallel to the layers) would give a theoretical expected interlayer distance of 15.9 Å (6.6 Å + 9.3 Å). This theoretical interlayer distance is only 0.3 Å larger than the distance experimentally measured by XRPD (15.6 Å). However, as we have previously observed for other intercalated ZrP materials (with intercalants such as $[Ru(bpy)_3]^{2+}$, PYMA, $[Ru(phend)_2bpy]^{2+}$, and MV^{2+})[42,54–56] ionic, hydrogen bonding, and other electrostatic interactions between the cations and the layers can cause the observed spacing to be somewhat smaller than those predicted from strictly van der Waals distances. In addition, it is possible that the intercalating molecules slightly interpenetrate the layers between the phosphate groups, thereby decreasing the interlayer spacing. The peak corresponding to about 10.6 Å at the highest loading level in Figure 2 corresponds to an available interlayer distance of 4.0 Å (10.6 Å–6.6 Å) for the intercalant. However, from the estimated dimer dimensions, it is improbable that the intact dimer can occupy a 4.0 Å interlayer distance.[57] To probe the origin of this peak at 10.6 Å, we intercalated separately the dmbpy and pyrazole ligands within the ZrP layers.[58] The XRPD patterns of dmbpy- and pyrazole-intercalated ZrP materials show maximum interlayer distances of 10.8–11.2 Å and 9.9 Å, respectively (Supporting Information, Figure S2). The obtained interlayer distances are in good agreement with previous reports of organic aromatic diamines,[59,60] amino acids,[61] and

dx.doi.org/10.1021/ic201423q | Inorg. Chem. 2012, 51, 2777–2784

other heterocyclic compounds[62] such as pyridine and quinoline intercalated in different ZrP phases. The calculated shortest dimensions of the platinum monomer (i.e., one subunit of the dimer), pyrazole, and dmbpy ligands are 4.1, 3.2, and 4.3 Å, respectively;[47] indicating that, if these molecules were to lie parallel to the ZrP layers, they would give interlayer distances ranging from 9.8 to 10.9 Å. While it is premature to make a definitive assignment, a possible explanation for the appearance of this peak at 10.6 Å at higher loading levels is dissociation of the dimer to form a monomer(s) and possibly free ligand(s).

X-ray Photoelectron Spectroscopy. Table 1 shows the Pt:P:N molar ratios of the $[\{Pt(dmbpy)(\mu\text{-}pz)\}_2]^{2+}$-exchanged ZrP materials as estimated from X-ray photoelectron spectroscopy (XPS) measurements. The XPS data show that the Pt:P molar ratios of the intercalated solids increase monotonically with an increase in the Pt:ZrP concentration ratio of the mixture used in their preparation. The 1:1 $[\{Pt(dmbpy)(\mu\text{-}pz)\}_2]^{2+}$:ZrP sample shows a Pt:P molar ratio of 1:11, which indicates that for each $[\{Pt(dmbpy)(\mu\text{-}pz)\}_2]^{2+}$ ion there are 5.5 ZrP formula units, corresponding to replacement of <10% of the exchangeable protons. To further assess whether $[\{Pt(dmbpy)(\mu\text{-}pz)\}_2]^{2+}$ had undergone any chemical change after the intercalation process, the Pt:N molar ratios were determined. The XPS data show that the Pt:N molar ratios of the intercalated solids increase monotonically with an increase in the Pt:ZrP concentration ratio of the mixture used in their preparation; the observed ratios depart from the expected theoretical ratio of 1:4.

Table 1. Platinum/Phosphorous/and Nitrogen Molar Ratios Obtained from XPS for $[\{Pt(dmbpy)(\mu\text{-}pz)\}_2]^{2+}$-Exchanged ZrP Samples

Pt:ZrP loading	Pt:P (XPS)	Pt:N (XPS)
1:1	1:11	1:3.4
1:5	1:13	1:3.5
1:10	1:17	1:3.7
1:25	1:18	1:3.9
1:30	1:22	1:3.8

These results are consistent with the notion that the $[\{Pt(dmbpy)(\mu\text{-}pz)\}_2]^{2+}$ dimers remain largely intact at lower loadings. The surface area occupied by one zirconium phosphate formula unit is 24 Å^2.[63] The dimer has an approximately triangular footprint, and the area projected on the ZrP layers by a $[\{Pt(dmbpy)(\mu\text{-}pz)\}_2]^{2+}$ ion positioned with the dmbpy ligand perpendicular to the ZrP layers is 54 Å^2. This gives a theoretical maximum loading of 0.44 $[\{Pt(dmbpy)(\mu\text{-}pz)\}_2]^{2+}$ ions per ZrP formula unit. From the XPS data the experimental maximum loading achieved is 0.22 $[\{Pt(dmbpy)(\mu\text{-}pz)\}_2]^{2+}$ ions per formula unit.

To assess the oxidation state of platinum, we performed high resolution XPS measurements at the Pt 4f region on the 1:1 $[\{Pt(dmbpy)(\mu\text{-}pz)\}_2]^{2+}$-exchanged ZrP blue-gray material. The spectrum shown in Figure 4 presents two sets of doublets, a major component with $4f_{7/2}$ and $4f_{5/2}$ peaks at 73.5 and 76.8 eV (90.4%) and a minor component at 71.3 and 74.6 eV (9.6%), confirming the presence of Pt in different oxidation states. The ratio of the $4f_{5/2}$ peak area to the $4f_{7/2}$ peak area in each doublet is 0.75, as expected from the degeneracy of the orbitals from which ionization occurs. To define the origin of the major and minor components in the XPS spectrum, we recorded the XPS spectrum of Pt foil, as well as that of the nonintercalated Pt(II) dimer complex (Table 2).

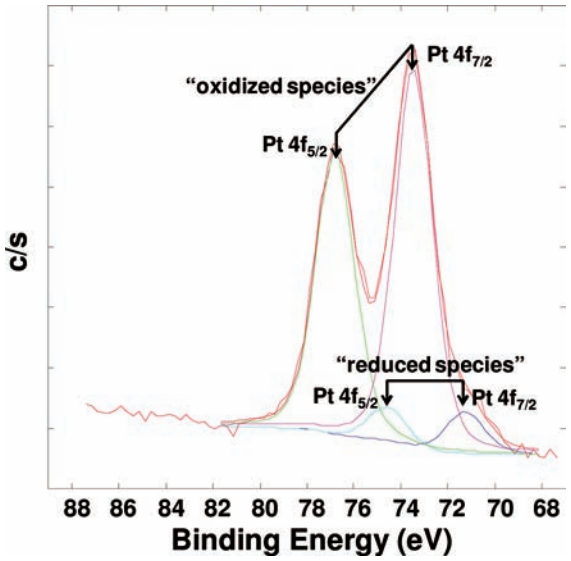

Figure 4. High resolution XPS spectrum for the blue-gray powder of 1:1 $[\{Pt(dmbpy)(\mu\text{-}pz)\}_2]^{2+}$-exchanged ZrP at the Pt 4f binding energy region. The red color spectrum represents the fitted curved of the individual function doublet peaks.

Table 2. High Resolution XPS Data: Binding Energies (eV) of Pt 4f Core Level of $[\{Pt(dmbpy)(\mu\text{-}pz)\}_2](BF_4)_2$ Complex and 1:1 $[\{Pt(dmbpy)(\mu\text{-}pz)\}_2]^{2+}$-Exchanged ZrP Materials

	binding energy (eV)	
material (color)	Pt $4f_{7/2}$	Pt $4f_{5/2}$
$[\{Pt(dmbpy)(\mu\text{-}pz)\}_2](BF_4)_2$ (yellow powder)	73.1	76.4
$[\{Pt(dmbpy)(\mu\text{-}pz)\}_2]^{2+}$-exchanged ZrP (blue-gray powder)	73.5	76.8
	71.3	74.6
$[\{Pt(dmbpy)(\mu\text{-}pz)\}_2]^{2+}$-exchanged ZrP (yellow-brown powder)	73.0	76.3
	71.9	75.2
Pt foil[60,61]	71.2	74.5

The data in Table 2 show that the binding energies of the peaks associated with the minor component in the intercalated ZrP are in excellent agreement with those of Pt metal, indicating partial reduction of the complex to give Pt(0) because of the reduction of some of the metal centers.[65,66] The obtained binding energies and areas for $[\{Pt(dmbpy)(\mu\text{-}pz)\}_2](BF_4)_2$ are in good agreement with those previously reported for Pt(II) complexes.[64,65] However, these energies are 0.4 eV less than those for the major component of the intercalated ZrP material. On the other hand, typical Pt 4f binding energies for Pt(IV) complexes are between 2 and 3 eV greater than their Pt(II) analogues.[28,65,67] Pt(III) 4f binding energies also are typically greater than the values obtained here, occurring in the 74.6−78.5 eV range.[25,35]

Therefore, the binding energies for the major component are consistent with an oxidation state intermediate between Pt(II) and Pt(III). In support of this interpretation, we present the binding energies of amidate-bridged tetramers[23,25] with average oxidation states of 2.25 (72.8 and 76.2 eV) and 2.5 (72.9 and 76.4 eV), as well as those of a platinum oxamate blue[68]

dx.doi.org/10.1021/ic201423q | Inorg. Chem. 2012, 51, 2777−2784

(Pt(2.25), 72.3 and 75.6 eV, 74.1 and 77.3 eV after deconvolution). Therefore, the binding energies for the blue-gray intercalated ZrP material are similar to the values obtained for this species with average oxidation states between 2 and 3. Thus, the XPS data are consistent with disproportionation of the Pt dimer within the heterogeneous chemical microenvironment of ZrP. The blue-gray color of the intercalated material also is consistent with this suggestion, since a blue color is characteristic of partial oxidation of the metal centers of "platinum blues".[22−24,34,36,69,70] The grayish tint may be explained by the presence of Pt metal.[71,72]

In an attempt to suppress this chemistry, the intercalation process was also carried out under two other conditions: (a) under a nitrogen gas stream atmosphere and (b) in the presence of $Na_2S_2O_4$. Dimer intercalation was insensitive to the nitrogen atmosphere, yielding a blue-gray color intercalated material. In contrast, a yellow-brown powder was obtained in the presence of $Na_2S_2O_4$. Similar to the blue-gray intercalated material, the high resolution XPS spectrum for this yellow-brown powder of 1:1 $[\{Pt(dmbpy)(\mu\text{-}pz)\}_2]^{2+}$-exchanged ZrP at the Pt 4f region also shows two sets of $4f_{7/2}$ and $4f_{5/2}$ doublets (Table 2 and Supporting Information, Figure S3). However, in contrast to the blue-gray intercalated material, the binding energies of the Pt 4f doublet at 73.0 and 76.3 eV corresponding to the major component (59% of the material) match those observed for the nonintercalated dimer, confirming at least partial suppression of the redox chemistry. A second Pt 4f doublet was also observed for the yellow-brown powder material at 71.9 and 75.2 eV (41% of the material), ~1 eV less than values for the nonintercalated Pt(II) dimer complex and 0.6 eV higher than for Pt(0). The binding energies for this minor component are unprecedented in the literature for Pt multinuclear complexes. We suggest that the oxidation state of the Pt metal center of the yellow-brown intercalated material obtained in the presence of the reducing agent is closer to +1.[73] Taken together, these results suggest that the ZrP microenvironment can accommodate a wide range of platinum oxidation states.

Absorption and Emission Spectroscopy. Figure 5a show the UV−visible absorption spectra of the blue-gray to light gray ethanol:water suspensions of the $[\{Pt(dmbpy)(\mu\text{-}pz)\}_2]^{2+}$-exchanged ZrP. The absorption bands are characteristically broad with a tailing long-wavelength profile attributed to scattered light. Nevertheless, absorption features can be distinguished which are consistent with bands observed in the spectrum of the dimer complex in fluid solution. Notably, vibronic structure in the 290−320 nm range matches the intense bipyridyl-centered spin-allowed $\pi-\pi^*$ transition (290sh, 306, 318 nm) observed in the UV−vis absorption spectrum of a 2.0×10^{-5} M $[\{Pt(dmbpy)(\mu\text{-}pz)\}_2]^{2+}$ ethanol:water solution. Similarly, the longer wavelength shoulder near 350 nm in the spectrum of the intercalated material, is in good agreement with the long-wavelength MLCT band maximizing at 343 nm in the spectrum of the dimer. As we have seen previously for intercalated platinum terpyridyl complexes[43] and other metal complexes,[42,55,74−76] the integrity of the complex is maintained, and we found no evidence of leaching of the intercalant to the solution.

To better assess the long-wavelength absorption properties of the $[\{Pt(dmbpy)(\mu\text{-}pz)\}_2]^{2+}$-exchanged ZrP samples, room-temperature diffuse reflectance spectra were recorded of the dimer salt in KBr (2%) and the intercalated materials at different loadings levels (Figure 5b).

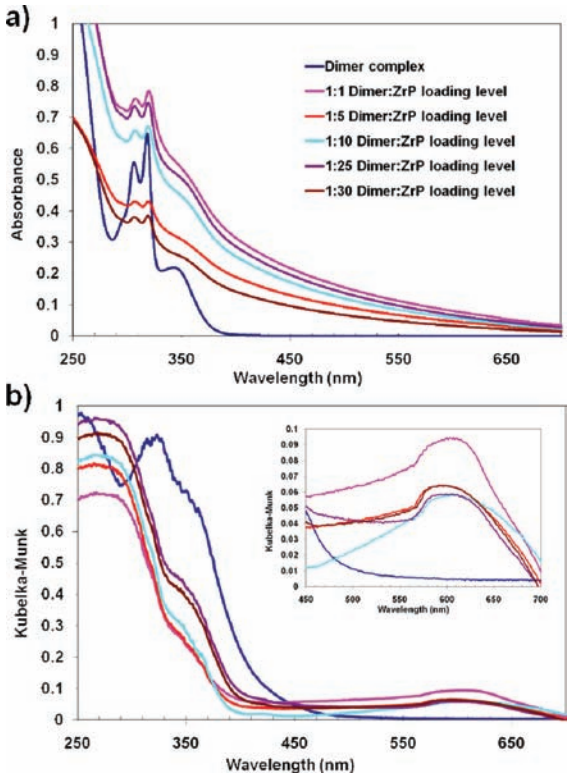

Figure 5. (a) UV−vis absorption spectra at room temperature of a 2.0×10^{-5} M $[\{Pt(dmbpy)(\mu\text{-}pz)\}_2]^{2+}$ ethanol:water solution and of $[\{Pt(dmbpy)(\mu\text{-}pz)\}_2]^{2+}$-exchanged ZrP ethanol:water suspensions (0.008% w/v) at different loading levels; (b) room-temperature diffuse reflectance spectra of $[\{Pt(dmbpy)(\mu\text{-}pz)\}_2](BF_4)_2$ in KBr (2%) and $[\{Pt(dmbpy)(\mu\text{-}pz)\}_2]^{2+}$-exchanged ZrP at different loadings levels. The inset shows the long wavelength region.

The spectrum of the pale yellow powder shows two broad absorption bands at 250 and 315 nm, and a shoulder near 350 nm with a long absorption tail until 450 nm. These are not features characteristic of metal−metal or intermolecular interactions. The diffuse reflectance spectra of the blue-gray $[\{Pt(dmbpy)(\mu\text{-}pz)\}_2]^{2+}$-exchanged ZrP materials show a broad absorption band from 250 to 300 nm and a shoulder near 350 nm. In addition, a long-wavelength absorption band appears at 600 nm and is absent from both the spectra of these materials in fluid solutions and the diffuse reflectance spectrum of the dimer salt (Inset Figure 5b). Similar results have been observed for "platinum blues" in which the blue color arises from absorptions in the 550−800 nm region. This absorption has been attributed to a mixed-valence transition between metal centers in different oxidation states.[33,36,69,70,77] Santiago et al. reported the appearance of a long-absorption band at 619 nm from powders produced in the intercalation reaction of ferrocene with ZrP; the band was attributed to the acidic microenvironment of ZrP inducing the formation of ferrocenium in the intercalation reaction.[55] The presence of the long-wavelength absorption band in the spectrum of the blue-gray intercalated ZrP material is consistent with our XPS results for the intercalated material (Figure 4) which suggested the presence of platinum metal in an oxidation state between Pt(II) and Pt(III).

$[\{Pt(dmbpy)(\mu\text{-}pz)\}_2]^{2+}$ is nonemissive in room-temperature fluid solution, but gives rise to intense structured blue-green emission from 4:1 ethanol/methanol glassy solution at 77

dx.doi.org/10.1021/ic201423q | Inorg. Chem. 2012, 51, 2777−2784

K (Figure 6a). The emission spectrum shows maxima at 453, 487, 512, and 524, with two shoulders near 555 and 605 nm.

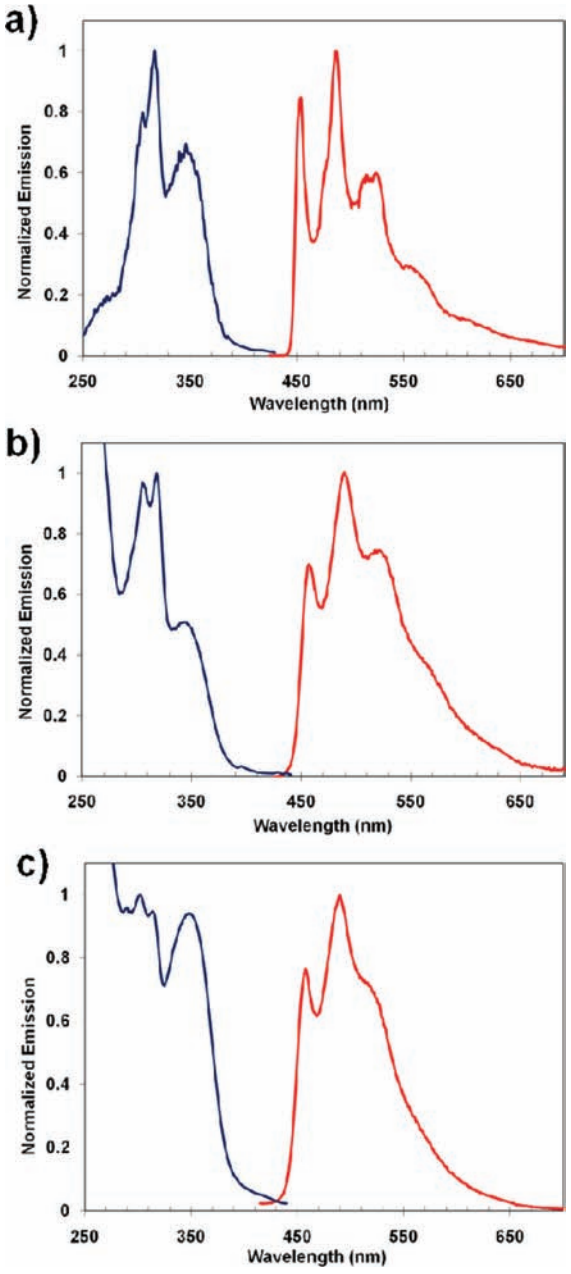

Figure 6. (**a**) Normalized emission (λ_{ex} = 318 nm) and excitation (λ_{em} = 455 nm) spectra of $[\{Pt(dmbpy)(\mu\text{-}pz)\}_2](BF_4)_2$ in 4:1 glassy ethanol/methanol at 77 K; (**b**) 1:1 $[\{Pt(dmbpy)(\mu\text{-}pz)\}_2]^{2+}$-exchanged ZrP from ethanol:water suspensions (0.008% w/v) and (**c**) powders at room temperature.

The resulting excitation spectrum from the glassy solution at 77 K shows bands at 306, 317, and 343 nm. The 1:1 $[\{Pt(dmbpy)(\mu\text{-}pz)\}_2]^{2+}$-exchanged ZrP materials are brightly emissive at room temperature in colloidal ethanol:water suspensions or as powders (Figures 6b and 6c). Both media show vibronically structured emissions from the intercalated materials similar to the dimer in glassy solution at 77 K. The resulting excitation spectra are in excellent agreement with the absorption spectra of dilute fluid solutions of the platinum salt and suspensions of the $[\{Pt(dmbpy)(\mu\text{-}pz)\}_2]^{2+}$-exchanged ZrP (Figure 5a), as well as the diffuse reflectance spectra of the dimer salt and powders intercalated materials (Figure 5b). The emission intensity of $[\{Pt(dmbpy)(\mu\text{-}pz)\}_2]^{2+}$-intercalated ZrP materials at different loading levels decreases with increasing Pt loading level. The observed emission from powders and suspensions of $[\{Pt(dmbpy)(\mu\text{-}pz)\}_2]^{2+}$-exchanged ZrP at room-temperature are consistent with the rigidochromic effect,[78] enforced by the more rigid environment of the layered exchanged material.

The emission profiles of the dimer glassy solution and $[\{Pt(dmbpy)(\mu\text{-}pz)\}_2]^{2+}$-exchanged ZrP materials bear an approximate mirror image relationship to the spin-allowed $\pi-\pi^*$ absorption band with vibronic structures consistent with bipyridine ligand modes in the 800−1600 cm^{-1} range.[8,79−81] These observations suggest that the metal−metal interaction is too weak to result in a lowest emissive MMLCT state. Our results suggest that emissions from the colloidal suspensions and powders of $[\{Pt(dmbpy)(\mu\text{-}pz)\}_2]^{2+}$-exchanged ZrP materials arise from a lowest predominantly spin-forbidden $\pi-\pi^*$ excited state centered on the bipyridine ligand, as noted for closely related compounds.[8,81,82]

Conclusions. The intercalation of $[\{Pt(dmbpy)(\mu\text{-}pz)\}_2]^{2+}$ into ZrP occurs by ion-exchange. The intercalant is likely held between the ZrP negatively charged layers by electrostatic interactions. In suspensions, there is no evidence of leaching of the intercalant to the solution. Zirconium phosphate layers promote the formation of a wide range of platinum oxidation states incorporated in a rigid-framework matrix. The intercalation reaction is accompanied by disproportionation to give Pt(0) and a product(s) with Pt in an oxidation state between 2 and 3. Diffuse reflectance from powders of the blue-gray intercalated materials show the formation of a low-energy band that is not present in the platinum dimer salt, supporting the presence of other platinum species. Use of dithionite in the synthesis largely suppresses oxidation of the complex. The $[\{Pt(dmbpy)(\mu\text{-}pz)\}_2]^{2+}$ complex is nonemissive in room-temperature fluid solution, but gives rise to intense blue-green emission in 77 K frozen glassy solution, characteristic of a lowest ligand-centered excited state. These observations suggest that the metal−metal interaction remains weak in the layered ZrP framework. Similarly, powders and colloidal suspensions of $[\{Pt(dmbpy)(\mu\text{-}pz)\}_2]^{2+}$-exchanged ZrP materials are brightly emissive at room temperature. The incorporation and behavior of this type of platinum system within the ZrP layers exhibits potential applications in many fields, such as chemosensors, photocatalysts, anticancer drugs delivery, and organic light emitting devices (OLEDs). Future efforts will focus on exploring the powder and solution properties of these novel materials by EPR, as well as kinetic investigations using ^{195}Pt NMR and ^{35}P NMR.

■ ASSOCIATED CONTENT

Ⓢ Supporting Information

FT-IR spectra of the dimer intercalated materials, XPS spectra of the yellow-brown dimer material, and XRPD patterns of pyrazole and dmbpy ligands in ZrP were included in PDF format. This material is available free of charge via the Internet at http://pubs.acs.org.

■ AUTHOR INFORMATION

Corresponding Author

*E-mail: jorge.colon10@upr.edu. Phone: (787) 764-0000, ext. 3220. Fax: (787) 756-8242.

Notes

The authors declare no competing financial interest.

■ ACKNOWLEDGMENTS

We thank the National Science Foundation (CHE-0134975) for their generous support. Special thanks to Dr. Edgar Resto and the staff of UPR's Material Characterization Center for their help with the XRPD and XPS measurements, and Dr. Angel Martí at Rice University for providing access to his spectroscopy instruments, helpful discussions, and technical assistance.

■ REFERENCES

(1) Kickelbick, G. *Hybrid Materials: Synthesis, Characterization, and Applications*; Wiley-VCH: Weinheim, Germany, 2007; Chapters 1, 4, and 8.
(2) Gómez-Romero, P.; Sanchez, C. *Functional Hybrid Materials*; Wiley-VCH: Weinheim, Germany, 2004; Chapters 1, 2, and 8.
(3) Minghetti, G.; Banditelli, G. *J. Chem. Soc., Dalton Trans.* **1979**, 1851−1856.
(4) Bailey, J. A.; Miskowski, V. M.; Gray, H. B. *Inorg. Chem.* **1993**, *32*, 369−370.
(5) Jain, V. K.; Kannan, S.; Tiekink, E. R. T. *J. Chem. Soc., Dalton Trans.* **1993**, 3625−3628.
(6) Lai, S. W.; Chan, C. W.; Cheung, T. C.; Peng, S. M.; Che, C. M. *Inorg. Chem.* **1999**, *38*, 4046−4055.
(7) Lai, S. W.; Chan, C. W.; Cheung, K. K.; Peng, M.; Che, C. M. *Organometallics* **1999**, *18*, 3991−3997.
(8) Connick, W. B.; Miskowski, V. M.; Houlding, V. H.; Gray, H. B. *Inorg. Chem.* **2000**, *39*, 2585−2592.
(9) Bandini, A. L.; Banditelli, G.; Bovio, B. *Polyhedron* **2001**, *20*, 2869−2875.
(10) Tam, A. Y.-Y.; Tsang, D.; Chan, M.-Y.; Zhu, N.; Yam, V. W.-W. *Chem. Commun.* **2011**, *47*, 3383−3385.
(11) Lu, W.; Mi, B. X.; Chan, M. C. W.; Hui, Z.; Che, C. M.; Lee, S. T. *J. Am. Chem. Soc.* **2004**, *126*, 4958−4971.
(12) Ma, B.; Li, J.; Djurovich, P.; Yousuffudin, M.; Bau, R.; Thompson, M. E. *J. Am. Chem. Soc.* **2005**, *127*, 28−29.
(13) Ma, B.; Djurovich, P.; Garon, S.; Alleyne, B.; Thompson, M. E. *Adv. Funct. Mater.* **2006**, *16*, 2438−2446.
(14) Chang, S. Y.; Chen, J. L.; Chi, Y.; Cheng, Y. M.; Lee, G. H.; Jiang, C. M.; Chou, P. T. *Inorg. Chem.* **2007**, *46*, 11202−11212.
(15) Williams, J. A. G.; Develay, S.; Rochester, D. L.; Murphy, L. *Coord. Chem. Rev.* **2008**, *252*, 2596−2611.
(16) Sakai, K.; Ozawa, H. *Coord. Chem. Rev.* **2007**, *251*, 2753−2766.
(17) Sun, R. W.-Y.; Chow, A. L.-F.; Li, X.-H.; Yan, J.; Chui, S. S.-Y.; Che, C.-M. *Chem. Sci.* **2011**, *2*, 728−736.
(18) Sakai, K.; Tomita, Y.; Ue, T.; Goshima, K.; Ohminato, M.; Tsubomura, T.; Matsumoto, K.; Ohmura, K.; Kawakami, K. *Inorg. Chim. Acta* **2000**, *297*, 64−71.
(19) Li, K.; Chen, Y.; Lu, W.; Zhu, N.; Che, C.-M. *Chem.—Eur. J.* **2011**, *17*, 4109−4112.
(20) Kui, S. C. F. C.; Chui, S. S.-Y.; Che, C.-M.; Zhu, N. *J. Am. Chem. Soc.* **2006**, *128*, 8297−8309.
(21) Che, C. M.; Fu, W.; Lai, S. W.; Hou, Y.; Liu, Y. L. *J. Chem. Soc.; Chem. Commun.* **2003**, 118−119.
(22) Matsumoto, K.; Sakai, K. *Adv. Inorg. Chem.* **2000**, *49*, 375−427.
(23) Sakai, K.; Takeshita, M.; Tanaka, Y.; Ue, T.; Yanagisawa, M.; Kosaka, M.; Tsubomura, T.; Ato, M.; Nakano, M. *J. Am. Chem. Soc.* **1998**, *120*, 11353−11363.
(24) Sakai, K.; Tanaka, Y.; Tsuchiya, Y.; Hirata, K.; Tsubomura, T.; Iijima, S.; Bhattacharjee, A. *J. Am. Chem. Soc.* **1998**, *120*, 8366−8379.
(25) Matsumoto, K.; Sakai, K.; Nishio, K.; Tokisue, Y.; Ito, R.; Nishide, T.; Shichi, Y. *J. Am. Chem. Soc.* **1992**, *114*, 8110−8118.
(26) O' Halloran, T. V.; Mascharak, P.; Williams, I.; Roberts, M.; Lippard, S. J. *Inorg. Chem.* **1987**, *26*, 1261−1270.
(27) O' Halloran, T. V.; Roberts, M.; Lippard, S. J. *Inorg. Chem.* **1986**, *25*, 957−964.
(28) Arrizabalaga, P.; Castan, P.; Laurent, J. *J. Am. Chem. Soc.* **1984**, *106*, 1300−1303.
(29) Hollis, L. S.; Lippard, S. J. *Inorg. Chem.* **1983**, *22*, 2605−2614.
(30) Matsumoto, K.; Takahashi, H.; Fuwa, K. *Inorg. Chem.* **1983**, *22*, 4086−4090.
(31) Matsumoto, K.; Fuwa, K. *J. Am. Chem. Soc.* **1982**, *104*, 897−898.
(32) Hollis, L. S.; Lippard, S. J. *J. Am. Chem. Soc.* **1981**, *103*, 6761−6763.
(33) Barton, J. K.; Caravana, C.; Lippard, S. J. *J. Am. Chem. Soc.* **1979**, *101*, 7269−7277.
(34) Barton, J. K.; Szalda, D. J.; Rabinowitz, H. N.; Waszczak, J. V.; Lippard, S. J. *J. Am. Chem. Soc.* **1979**, *101*, 1434−1441.
(35) Barton, J. K.; Best, S. A.; Lippard, S. J.; Walton, R. A. *J. Am. Chem. Soc.* **1978**, *100*, 3785−3788.
(36) Barton, J. K.; Rabinowitz, H. N.; Szalda, D. J.; Lippard, S. J. *J. Am. Chem. Soc.* **1977**, *99*, 2827−2829.
(37) Brown, D. B.; Burbank, R. D.; Robin, M. B. *J. Am. Chem. Soc.* **1969**, *91*, 2895−2902.
(38) Sakai, K.; Sato, T.; Tsubomura, T.; Matsumoto, K. *Acta Crystallogr., Sect. C* **1996**, *52*, 783−786.
(39) Clearfield, A.; Duax, W. L.; Medina, A. S.; Smith, G. D.; Thomas, J. R. *J. Phys. Chem.* **1969**, *73*, 3424−3430.
(40) Clearfield, A.; Landis, A. L.; Medina, A. S.; Troup, J. M. *J. Inorg. Nucl. Chem.* **1973**, *35*, 1099−1108.
(41) Kijima, T. *Bull. Chem. Soc. Jpn.* **1982**, *55*, 3031−3032.
(42) Martí, A.; Colón, J. L. *Inorg. Chem.* **2003**, *42*, 2830−2832.
(43) Rivera, E. J.; Figueroa, C.; Grove, L. J.; Connick, W. B.; Colón, J. L. *Inorg. Chem.* **2007**, *46*, 8569−8576.
(44) Jenkins, R.; Snyder, R. L. *Introduction to X-Ray Diffractometry*; John Wiley and Sons: New York, 1996.
(45) Costantino, U. *J. Chem. Soc., Dalton Trans.* **1979**, 402−405.
(46) Backov, R.; Bonnet, B.; Jones, D. J.; Roziere, J. *Chem. Mater.* **1997**, *9*, 1812−1818.
(47) As calculated using the SPARTAN Student Physical-Chemistry Edition for Windows, version 1.0.1, Wave function, using a semiempirical model with a RHF/PM3 as a basis set.
(48) Bailey, J. A.; Gray, H. B. *Acta Crystallogr., Sect. C* **1992**, *48*, 1420−1422.
(49) Komeda, S.; Ohishi, H.; Yamane, H.; Harikawa, M.; Sakaguchi, K. I.; Chikuma, M. *J. Chem. Soc., Dalton Trans.* **1999**, 2959−2962.
(50) Chiu, B. K.; Lam, M. H. W.; Lee, D.; Wong, W. *J. Organomet. Chem.* **2004**, *689*, 2888−2899.
(51) Goel, A. B.; Goel, S.; Vanderveer, D. *Inorg. Chim. Acta* **1984**, *82*, L9−L10.
(52) Kukushkin, V. Y.; Aleksandrova, E. A.; Leovac, V. M.; Ivegeimage, E. Z.; Belsky, V. K.; Konovalov, V. E. *Polyhedron* **1992**, *11*, 2691−2696.
(53) Yang, C.; Clearfield, A. *React. Polym., Ion Exch., Sorbents* **1987**, *5*, 13−21.
(54) Bermúdez, R. A.; Colón, Y.; Tejada, G. A.; Colón, J. L. *Langmuir* **2005**, *21*, 890−895.
(55) Santiago, M.; Declet-Flores, C.; Diaz, A.; Velez, M.; Bosques, M.; Sanakis, Y.; Colón, J. L. *Langmuir* **2007**, *23*, 7810−7817.
(56) Martí, A.; Paralitici, G.; Maldonado, L.; Colón, J. L. *Inorg. Chim. Acta* **2007**, *360*, 1535−1542.
(57) As calculated using the SPARTAN Student Physical-Chemistry Edition for Windows, version 1.0.1, Wave function, using a semiempirical model with a RHF/PM3 as a basis set. The calculated width with the bpy ligand parallel to the ZrP layers is 4.1 Å.
(58) The intercalation of the ligands (at a 1:1 ligand:ZrP molar ratio) were obtained using the same procedure shown in the Experimental Section. XRPD patterns were obtained using a Siemens D5000 powder diffractometer.
(59) Ferragina, C.; Cafarelli, P.; De Stefanis, A.; Mattei, G. *Mater. Res. Bull.* **1999**, *34*, 1039−1053.
(60) Ferragina, C.; La Ginestra, A.; Massucci, M. A.; Patrono, P.; Tomlinson, A. *J. Phys. Chem.* **1985**, *89*, 4762−4769.
(61) Costantino, U.; Massucci, M. A.; La Ginestra, A.; Tarola, A. M.; Zampa, L. *J. Incl. Phenom.* **1986**, *4*, 147−162.

(62) Hasegawa, Y.; Akimoto, T.; Kojima, D. *J. Incl. Phenom. Mol. Recognit. Chem.* **1995**, *20*, 1−12.
(63) Clearfield, A. *Prog. Inorg. Chem.* **1998**, *47*, 371−510.
(64) Riggs, W. M. *Anal. Chem.* **1972**, *44*, 830−832.
(65) Cahen, D.; Lester, J. E. *Chem. Phys. Lett.* **1973**, *18*, 108−110.
(66) Wagner, C. D.; Riggs, W. M.; Davis, L. E.; Moulder, J. F.; Muilenberg, G. E. *Handbook of X-Ray Photoelectron Spectroscopy*; Perkin-Elmer Corp.: Eden Prairie, MN, 1979.
(67) Burroughs, P.; Hamnet, A.; McGlip, J. F.; Orchard, A. F. *J. Chem. Soc., Faraday Trans. 2* **1975**, *71*, 177−187.
(68) Burness, J. H. *Inorg. Chim. Acta* **1980**, *44*, L49−L51.
(69) Chang, C. A.; Marcotte, R. B.; Patterson, H. H. *Inorg. Chem.* **1981**, *20*, 1632−1636.
(70) Flynn, C. M.; Viswanathan, T. S.; Martin, B. *J. Inorg. Nucl. Chem.* **1977**, *39*, 437−439.
(71) Dokoutchaev, A.; Krishnan, V. V.; Thompson, M. E.; Balasubramanian, M. *J. Mol. Struct.* **1998**, *470*, 191−205.
(72) Byrd, H.; Clearfield, A.; Poojary, D.; Reis, K. P.; Thompson, M. E. *Chem. Mater.* **1996**, *8*, 2239−2246.
(73) Palmans, R.; MacQueen, D. B.; Pierpont, C. G.; Frank, A. J. *J. Am. Chem. Soc.* **1996**, *118*, 12647−12653.
(74) Martí, A.; Rivera, N.; Soto, K.; Maldonado, L.; Colón, J. L. *Dalton Trans.* **2007**, 1713−1718.
(75) Santiago, M.; Velez, M.; Borrero, S.; Diaz, A.; Casillas, C.; Hoffman, C.; Guadalupe, A.; Colón, J. L. *Electroanalysis* **2006**, *18*, 559−572.
(76) Martí, A.; Colón, J. L. *Inorg. Chem.* **2010**, *49*, 7298−7303.
(77) Appleton, T. G.; Berry, R. D.; Hall, J. R. *Inorg. Chim. Acta* **1982**, *64*, L229−L233.
(78) Wrighton, M.; Morse, D. L. *J. Am. Chem. Soc.* **1974**, *96*, 998−1003.
(79) Miskowski, V. M.; Houlding, V. H.; Che, C. M.; Wang, Y. *Inorg. Chem.* **1993**, *32*, 2518−2524.
(80) Miskowski, V. M.; Houlding, V. H. *Inorg. Chem.* **1991**, *30*, 4446−4452.
(81) Miskowski, V. M.; Houlding, V. H. *Inorg. Chem.* **1989**, *28*, 1529−1533.
(82) Fleeman, W. F.; Connick, W. B. *Comments Inorg. Chem.* **2002**, *23*, 205−230.